Platinum(II) and Phosphorus MM3 Force Field Parametrization for Chromophore Absorption Spectra at Room Temperature

ARTICLE *in* THE JOURNAL OF PHYSICAL CHEMISTRY A · MARCH 2010

Impact Factor: 2.69 · DOI: 10.1021/jp911046u · Source: PubMed

3 AUTHORS, INCLUDING:

Jonas Sjöqvist

6 PUBLICATIONS **19** CITATIONS

SEE PROFILE

Mathieu Linares

Linköping University

63 PUBLICATIONS **978** CITATIONS

SEE PROFILE

Platinum(II) and Phosphorus MM3 Force Field Parametrization for Chromophore Absorption Spectra at Room Temperature

Jonas Sjöqvist, Mathieu Linares, and Patrick Norman*

Department of Physics, Chemistry and Biology, Linköping University, SE-581 83 Linköping, Sweden

Received: November 20, 2009; Revised Manuscript Received: February 23, 2010

Platinum(II) and phosphine MM3 force field parameters are derived from fits to the ground state potential energy surface at the level of Kohn−Sham density functional theory with employment of the B3LYP exchange-correlation functional. The parametrization includes bond stretch, angle bend, and torsional parameters for a planar platinum(II) center with phosphine and ethynyl ligands. The force field is used to study the dynamics of a fifth-generation dendrimer-coated platinum(II)organic compound in tetrahydrofurane solution at room temperature, and, based on a selection of conformations from the molecular dynamics simulation, the averaged linear absorption spectrum is determined with use of the CAM-B3LYP functional. The main absorption peak in the theoretical absorption spectrum is found at a transition wavelength of 325 nm with a full-width at half-maximum of 26 nm due to conformational broadening.

I. Introduction

Over the past 15 years, there have appeared a large number of publications in the literature devoted to the study of fundamental spectroscopic as well as electronic and photonic properties of π-conjugated platinum(II) organometallic systems.[1−37] The list of references is extensive yet not exhaustive, and it reflects the various interests that research groups have in this class of compounds. A common set of properties can be identified for molecules belonging to this class, and it is the employment of one or several of these properties that opens the door to a number of technical applications. The electronic ground states of these molecules are of singlet spin symmetry with a gap energy large enough to make the materials quite transparent (sometimes yellowish in color). The first broad absorption band in the near-ultraviolet region strongly dominates the linear absorption spectra, and due to the internal heavy-atom effect there is a very high probability (90−100%) that, upon absorption, the system will undergo a ultrafast intersystem crossing and end up in the triplet manifold of states.[2,19] Both the nonradiative and phosphorescence lifetimes vary strongly depending on ligands, environment, and concentrations,[21] but the time scale is such that triplet exciton transport is observed.[10] It is also recognized that excited state absorption in the triplet manifold states is a key absorption channel in nano- and picosecond pulsed laser spectroscopy.[2] From a material processing and device production point of view, there are issues such as structural, chemical, mechanical, and thermal stability to be considered. It has been demonstrated that stable inorganic and organic glass materials can be processed with incorporation of platinum(II) chromophores.[29] Diverse ligand substitutions allow the optical characteristics of these chromophores to be fine-tuned. Applications based on platinum(II) compounds include photosensitizers,[25] multielectron transfer,[24] solar cells,[30,35] light emitting diodes,[32−34] and optical power limiting.[11,29]

Regardless of the application, when it comes to the stage of optimizing the performance of the material against a set of key electronic and/or optical properties, there is a need for a mix of basic understanding and trial-and-error activities. It is of course desirable to minimize the need of the latter, not only from a labor-cost perspective but also by arguments of scientific appeal, and the main tools at hand to reach a basic understanding are spectroscopy and theory. We believe that theory constitutes an indispensable ingredient in this work with an ability to resolve the spectrum of states and address individual coupling elements between them. Electronic structure calculations based on density functional theory (DFT) are carried out both in support to experimental work[4,6,14,15,17,21,28] as well as on a stand-alone basis.[3,5,12,16,18,37] The quantum mechanical results have also been coupled to a time- and space-resolved electrodynamical model in order to determine the laser pulse propagation through optically absorbing materials, and thereby achieve simulations of the device performance rather than mere chromophore characterization.[5,12,16] Such simulations show that, in the visible region, the predominant light-harvesting is accomplished via excited state absorption but that the nonresonant linear absorption in the ground state is important to initiate the process.

Among the approximations made in the theoretical work, the most striking one is the adoption of zero temperature conditions with molecular conformations corresponding to the global minima of the potential energy surfaces. The electronic π-conjugation is in this case optimum and the optical responses are at maximum. This situation is in stark contrast to the conditions of the experiment (room temperature) where low torsional barriers cause free rotation and breaking of the conjugation. It is our intention to address this issue in the present work and to introduce classical molecular mechanics based on force fields. Due to the nature of our molecular system we have chosen to base our work on the MM3 force field by Allinger,[38] where specific consideration has been paid to the parametrization of conjugated hydrocarbon systems.[39] We will contribute to this force field the parameters of the planar platinum(II) center with phosphine and ethynyl ligands, and, from the resulting molecular dynamics (MD) simulations, we will extract molecular conformation snapshots to be used in subsequent quantum chemical calculations of the optical responses. This follows, in essence, the strategies of Calus et al.[40] and Kongsted et al.[41] that were used in simulations of one- and two-photon absorption spectra,

* To whom correspondence should be addressed. E-mail: panor@ifm.liu.se.

10.1021/jp911046u
Published on Web 03/19/2010

respectively. In this manner, we will obtain theoretical absorption spectra that include the effects of conformational broadening and, as mentioned, the accompanying reduction in π -conjugation. As an example system we choose to study one of the simplest platinum(II)−acetylides, but, since almost all of the referred to platinum(II) organic systems share an identical heavy-atom center, the derived force field parameters can be quite generally used.

II. Methodological Approach

A. Molecular Dynamics. The MM3 force field is separated into nine kinds of interactions and takes the form

$$E = E_s + E_\theta + E_\omega + E_{vdw} + E_{el} + E_{oop} + E_{s\theta} + E_{\omega s} + E_{\theta\theta'} \quad (1)$$

where the first three are the main bonded interactions referred to as bond stretch, angle bend, and torsion, respectively. The next two terms denote nonbonded interactions referred to as van der Waals and electrostatic interactions. It is noted that E_{vdw} contains, in addition to the long-range dispersive interaction between atoms, also the short-range repulsive part, and E_{el} is parametrized as bond dipole interaction. The remaining four terms refer to bonded interactions that are of lesser concern for the parametrization of the platinum(II) center, and they are known as out-of-plane bending, stretch−bend, torsion−stretch, and bend−bend interactions, respectively.

The planar platinum(II) center is quite rigid and will be parametrized by use of the three main bonded interactions E_s, E_θ, and E_ω. The explicit form of the bond stretch interaction in the MM3 force field is given by

$$E_s = 143.88\frac{k_s}{2}(l - l_0)^2\left[1 - 2.55(l - l_0) + \frac{7}{12}2.55(l - l_0)^2\right] \quad (2)$$

where l is the distance between two atoms, l_0 is an equilibrium bond length, and k_s is the corresponding force constant. The lengths are given in angstroms, the force constant in mdyn/Å, and the energy in kcal/mol. The angle bending interactions are parametrized by the expression

$$E_\theta = 0.043828\frac{k_\theta}{2}(\theta - \theta_0)^2[1 - 0.014(\theta - \theta_0) + 5.6 \times 10^{-5}(\theta - \theta_0)^2 - 7.0 \times 10^{-7}(\theta - \theta_0)^3 + 9.0 \times 10^{-10}(\theta - \theta_0)^4] \quad (3)$$

where θ is the angle formed by three atoms, θ_0 is the equilibrium angle, and k_θ is the corresponding force constant. The energy is again given in kcal/mol, with angles given in degrees and the force constant given in mdyn·Å/rad^2. Finally, the torsion interactions take the form

$$E_\omega = \frac{V_1}{2}(1 + \cos\omega) + \frac{V_2}{2}(1 - \cos 2\omega) + \frac{V_3}{2}(1 + \cos 3\omega) \quad (4)$$

where the force constants V_1, V_2, and V_3 (and thus the energy) are given in kcal/mol, and ω is the dihedral angle for a set of four atoms.

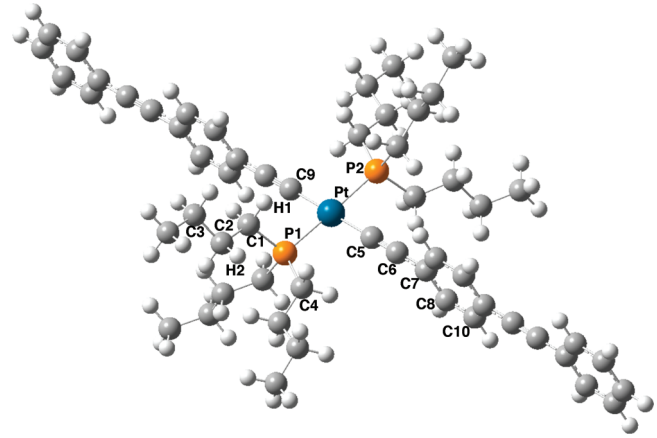

Figure 1. Molecular structure of the Pt1 chromophore. Atoms relevant to the parametrization in the MM3 force field are labeled.

In the MM3 force field model, atoms are divided into types depending not only on the element in question but also its hybridization: sp^3-, sp^2-, and sp-bonded carbons are defined as types 1, 2, and 4, respectively, and hydrogen is defined as type 5. The molecular structure of our platinum(II) acetylide system, which henceforth will be abbreviated by Pt1, is depicted in Figure 1. Platinum and phosphorus in this molecular configuration will be referred to as types 384 and 360, respectively, and all force field parameters involving either of these atoms will need to be determined. In addition, we will introduce separate atom types for the phenyl carbons, labeled by C7 and C8 in Figure 1, to account for the bond length alternation (we will define these carbon types as 385 and 386, respectively). For these carbon types we will parametrize the three bond stretch parameters 385−4, 385−386, and 386−386 (although the force constant of 386−386 is set equal to that of 385−386) as well as the angle bend parameter 4−385−386. All other needed parameters that include the types 385 and 386 are taken from the equivalent parameters for type 2. All things considered, there are 6 bond stretch, 9 angle bend, and 11 torsion parameters to be determined.

The needed parameters are determined by fitting the total force field energy to the potential energy surface obtained from first-principles DFT with use of the hybrid B3LYP exchange correlation functional.[42] This fitting procedure is carried out for the parameters associated with one bond stretch, angle bend, or torsion parameter at a time. It is, however, recognized that two of the angle bend parameters are interdependent (i.e., changing one angle will also change the other), namely 1−360−1 and 384−360−1, and the fittings of these parameters are carried out simultaneously.

Out of the 11 torsional parameters to be determined, 5 are given by the symmetry of the planar platinum(II) center. For the 4 torsional angles 384−4−4−385, 4−384−4−4, 360−384−4−4, and 360−384−360−1, at least 3 of the involved atoms are linear in the optimized structure. For these sets of four atoms, twisting them any amount about the central bond produces a structure identical to the initial one, and the torsional barriers must therefore equal to zero. Arguments of symmetry can also be applied to the torsional parameter 4−384−360−1. There are two sp-carbons bonded to Pt in a C_2 symmetry formation and there are three sp^3-carbons bonded to each P in a C_3 symmetry formation, so there can only be contributions from the V_2- and V_3-terms in eq 4. Adding up contributions, the total energy from the 4−384−360−1 torsion will be independent of the rotation angle and equal to the constant value of $3V_2 + 3V_3$. For simplicity, we have chosen to

let this constant value be equal to zero by setting the value of both parameters equal to zero.

The remaining six torsional parameters that need to be determined are all interdependent to a degree that makes it impossible to perform a multidimensional fit. Instead we derive them by use of a set of auxiliary molecules so that the six parameters fully decouple. For the 384−360−1−5 parameter we study a variant of the Pt1 molecule where the 6 butyls are replaced by methyls. Changing 1 of these 6 methyls for $C(CH_3)_3$ allows for a determination of the torsional parameter 384−360−1−1. With use of the molecule trimethylphosphine we can determine the 5−1−360−1 parameter, and with the change of one methyl in trimethylphosphine for $C(CH_3)_3$ we can obtain the 1−1−360−1 parameter. The torsional parameter 5−1−1−360 is obtained with use of the molecule $CCH_3(PH_2)_3$, and, finally, the 1−1−1−360 parameter we determine from this molecule by changing the methyl for $C(CH_3)_3$.

B. Linear Absorption. The linear absorption spectrum of a randomly oriented molecular system is related to the oscillator strengths, and, leaving out any constants of proportionality, the absorption band associated with electronic state n is given by

$$\sigma^{0\rightarrow n}(\omega) \propto \sum_{\nu,\nu'} p_\nu f^{0,\nu\rightarrow n\nu'} g(\omega - \Delta\omega_{0,\nu}^{n,\nu'}) \propto \sum_{\nu,\nu'} p_\nu \Delta\omega_{0,\nu}^{n,\nu'} |\langle\nu|\boldsymbol{\mu}(R)|\nu'\rangle|^2 g(\omega - \Delta\omega_{0,\nu}^{n,\nu'}), \quad (5)$$

where ω is the angular frequency of the external electric field, and g is a line shape function centered at the transition frequency $\Delta\omega_{0,\nu}^{n,\nu'}$. Moreover, we have assumed that the initial state of the system is described by an incoherent ensemble of chromophores with populations in the set of vibrational states $|\nu\rangle$ of the electronic ground state $|0\rangle$ (the population probabilities are denoted by p_ν), and a summation is made over the vibrational states $|\nu'\rangle$ of the electronically excited state $|n\rangle$. A Born−Oppenheimer separation of electronic and vibrational degrees of freedom is also employed in arriving at the last equation.

The components of the electronic transition dipole moment $\mu_\alpha(R) = \langle 0(R)|\,\hat{\mu}_\alpha\,|n(R)\rangle$ are readily available from standard quantum chemical calculations, but the vibrational states are not, at least for a system such as ours with a large number of degrees of freedom. It is our intention to bypass the explicit reference to the vibrational states by use of MD trajectories, and, in doing so, a quantum description of the nuclear motions will be disregarded. From the MD trajectories a set of N snapshots are sampled out, and for which quantum chemical calculations of absorption spectra are performed, and, again ignoring constants of proportionality, we will determine the linear absorption spectrum according to

$$\sigma^{0\rightarrow n}(\omega) \approx \frac{1}{N}\sum_{i=1}^{N} \Delta\omega_0^n(R_i)|\boldsymbol{\mu}(R_i)|^2 g[\omega - \Delta\omega_0^n(R_i)] \quad (6)$$

For the line-shape function, we will employ a unit amplitude Gaussian with a half-width half-maximum (HWHF) line broadening of 0.1 eV, which, in the spectral region around 320 nm, corresponds to 8 nm.

III. Computational Details

All first-principles structure optimizations and energy calculations, needed for the parametrization of the MM3 force field, were carried out using the Gaussian program.[43] In this work, the B3LYP exchange-correlation functional[42] was used in conjunction with the 6-31G*[44,45] and 6-31G[44] all-electron basis sets for carbon and hydrogen, respectively, and the Stuttgart (SDD) relativistic effective core potentials (ECPs) for platinum[46] and phosphorus.[47] The scans of bond lengths were done for distances within ±0.2 Å of the equilibrium structure; the scans of bond angles were done for angles within ±5° of the equilibrium structure; and torsional angles were scanned over full 360° bond rotations.

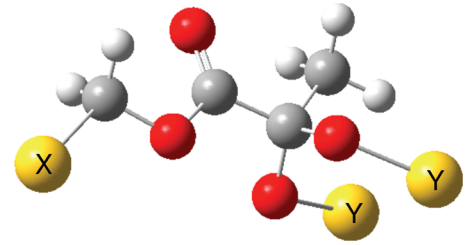

Figure 2. One generation of the dendrimer used to create the Pt1-G5 molecule. X indicates the point of attachment to a molecule or a previous generation of the dendrimer. Y indicates a point where the dendrimer is either continued with an additional generation or terminated.

All force field energy calculations and MD simulations were carried out with the Tinker program[48] using force field parameters from the MM3 set (parameters not available in this set are derived in the present work). The MD simulations were performed in the canonical ensemble at a temperature of 300 K using the Berendsen thermostat,[49] and they were run for a time period of 200 ps using an integrations step of 1 fs. Periodic boundary conditions were employed with 1 solute molecule, the fifth-generation dendrimer-coated version of Pt1 (referred to as Pt1-G5, with the dendrimer used shown in Figure 2), dissolved in a unit cell of size 35.9 × 35.9 × 76.9 $Å^3$ containing 585 solvent molecules (tetrahydrofurane, THF). The process of dissolving Pt1-G5 in THF was done by placing the chromophore into the unit cell of a thermally equilibrated pure liquid at a concentration of 0.89 g/cm^3 and by subsequent removal of solvent molecules overlapping with the chromophore. The chromophore concentration is in this case equal to 16.8 mmol/dm^3, which is in the range of concentrations considered in experiments.[21]

The calculations of absorption spectra were carried out with the Dalton program,[50] and they were based on time-dependent DFT with use of the Coulomb attenuated method B3LYP (CAMB3LYP) exchange correlation functional[51] as implemented by Peach et al.[52] In the calculations of spectra for the MD snapshots, we employed the 6-31G basis sets for carbon and hydrogen[44] and the SDD potentials[46,47] for Pt and P. A benchmark calculation of the basis set effects on the linear absorption spectra was carried out at the equilibrium geometry with use of Dunning's aug-cc-pVDZ[53] basis set for carbon. An estimate of the direct solvation effects on transition wavelengths was obtained by use of the nonequilibrium self-consistent reaction field model[54] employing a spherical cavity with a radius of 16.5 ± 0.2 Å, which corresponds to half of the largest interatomic distance in Pt1 in the set of 10 selected MD snapshots plus the van der Waals radius of 1.09 Å for hydrogen. The static and dynamic dielectric constants were chosen as equal to 7.58 and 1.971, in order to correspond to solvation in THF.

IV. Results and Discussion

A. Force Field Verifications. The optimized MM3 force field parameters are given in Table 1, and, taken one at a time,

TABLE 1: Optimized MM3 Force Field Parameters[a]

bond type	atoms	l_0 (Å)	k_s (mdyn/Å)
1−360	C1−P1	1.850	2.689
384−4	Pt−C5	2.019	2.563
384−360	Pt−P1	2.330	1.790
385−4	C7−C6	1.426	6.025
386−386	C8−C10	1.388	7.759
385−386	C7−C8	1.406	7.759
angle type	**atoms**	θ_0 (°)	k_θ (mdyn·Å/rad^2)
4−385−386	C6−C7−C8	121.1	0.70
1−1−360	C2−C1−P1	114.8	0.70
5−1−360	H1−C1−P1	105.2	0.47
1−360−1	C1−P1−C4	105.2	0.98
4−384−4	C5−Pt−C9	180.0	0.82
384−4−4	Pt−C5−C6	180.0	0.35
360−384−4	P1−Pt−C5	90.0	0.80
360−384−360	P1−Pt−P2	180.0	0.56
384−360−1	Pt−P1−C1	116.0	0.31
dihedral type	**atoms**	V_1 (kcal/mol)	V_2 (kcal/mol)	V_3 (kcal/mol)
1−1−360−1	C2−C1−P1−C4	0.000	0.000	0.712
1−1−1−360	C3−C2−C1−P1	0.000	0.000	0.600
5−1−1−360	H2−C2−C1−P1	0.000	0.000	0.400
5−1−360−1	H1−C1−P1−C4	0.000	0.000	0.386
384−4−4−385	Pt−C5−C6−C7	0.000	0.000	0.000
384−360−1−1	Pt−P1−C1−C2	0.000	0.000	1.400
384−360−1−5	Pt−P1−C1−H1	0.000	0.000	−0.330
4−384−4−4	C9−Pt−C5−C6	0.000	0.000	0.000
360−384−4−4	P1−Pt−C5−C6	0.000	0.000	0.000
4−384−360−1	C5−Pt−P1−C1	0.000	0.000	0.000
360−384−360−1	P2−Pt−P1−C1	0.000	0.000	0.000

[a] Atom numbering is made in accordance with Figure 1.

they represent close fits to the DFT/B3LYP potential energy surface for a given geometry distortion (bond stretch, angle bend, or torsion)—we provide plots of curve fits as Supporting Information. In combination, the MM3 force field parameters couple in intricate ways and it becomes relevant to compare the MM3-optimized structure to the B3LYP-optimized one in order to judge the performance of the force field. One single-number measure of the quality of the force field is obtained by determining the relaxation energy in the force field optimization, starting from the B3LYP-optimized structure and ending in the MM3-optimized one. For Pt1, this resulted in a relaxation energy of 13 kcal/mol, which, considering the large number of atoms in the molecule, is a very small number. We note that, in order to arrive at such a low relaxation energy, it is crucial to reparametrize some of the sp^2-carbons in the phenyls, as described in Section II. On the other hand, after this has been done, the relaxation energy is composed only of small contributions from a large number of small differences in the MM3- and B3LYP-optimized structures.

The only notable difference in the MM3-optimized structure (as compared to the B3LYP-optimized one) is a 90° rotation of the 2 phenyl rings closest to the platinum. This does not, however, represent a significant change in energy due to the fact that the rotational barrier for the phenyls is close to zero (also at the B3LYP level of theory[21]). This means that computed either with QM or MM methods, the phenyl rings would be rotating freely at room temperature, and their angles in the optimized structure is of no real importance.

One issue that becomes relevant in concern with the dynamics is whether the force field is accurate over the entire ranges of observed values of bond lengths and angles. Our scanning of bond lengths and angles was carried out for intervals of ±20 pm and ±5°, respectively, and these intervals should be contrasted with the ranges of bond parameter values at the temperature of interest. If we focus on the electron conjugation in the system, the bond length and angle of predominant importance are the Pt−C bond lengths and the P−Pt−C bond angles. At a temperature of 300 K, the standard deviations for the observed values of these two groups of parameters are 5 pm and 2.6°, respectively, which thus fall well within our scanning intervals.

TABLE 2: Transition Wavelengths and Oscillator Strengths for the $S_0 \rightarrow S_1$ Transition in Pt1 and Pt1−G1

molecule	geometry[a]	λ (nm)	f
Pt1	A	310	3.75
Pt1	B	316	1.96
Pt1	C	304	3.69
Pt1-G1	A	316	4.19

[a] A: B3LYP-optimized structure, B: MM3-optimized structure, C: MM3-optimized structure made planar.

Another measure of the quality of the force field parameters is given by a comparison of absorption spectra, obtained at the respective optimized geometries. If we focus attention on the dominating $S_0 \rightarrow S_1$ transition, we see a small red-shift of 6 nm in the spectrum for the MM3-optimized structure as compared to the spectrum for the B3LYP-optimized structure, see Table 2. On the other hand, it is found that the oscillator strength is nearly halved following the 90° rotation of the phenyl rings. This is of course a consequence of the breaking of the π-conjugation in the chromophore backbone, which has a strong impact on the optical responses. To make this clear, a new structure was created by turning the phenyl rings back to their original planar position but keeping the rest of the MM3-optimized structure frozen. The absorption spectrum obtained at this geometry (denoted by C in Table 2) shows an oscillator strength that is in close agreement with that obtained at the B3LYP-optimized structure (denoted by A in the same table). In conclusion, we estimate errors in transition wavelengths as introduced by the use of the MM3 force field to be within 10 nm, whereas the breaking of π-conjugation, which causes reduced spectral intensities, is a true effect at room temperature that will be correctly described by the dynamics simulations.

B. Other Model Approximations. Apart from the force field, there are several other computational issues to be considered in the determination of a linear absorption spectrum. With respect to the choice of exchange-correlation functional, it is important to properly describe the metal-to-ligand charge-transfer character of the electronic transitions, and, in the present work, we will employ the CAM-B3LYP functional as a result of previous experiences and results.[21] The 6-31G family of basis sets has, despite its small size, shown to perform fairly well in this respect—although with blue-shifts as compared to results obtained with high-quality basis sets.[21] In the present work, we give an illustration of this fact by the provision of two transition wavelengths of the $S_0 \rightarrow S_1$ transition obtained with, on the one hand, the 6-31G basis set and, on the other hand, with the aug-cc-pVDZ basis set (for carbon). The red-shift associated with the improvement in the basis set is seen in Table 3 to be 14.5 nm. This result corresponds to an average taken over 10 randomly selected snapshots of an MD trajectory. The standard deviation of the red-shift is as small as 1.9 nm, which means that the basis set error is quite systematic and can be accounted for by the application of an overall spectral shift. Since we are to determine a large number of snapshot spectra, we will adopt this strategy.

TABLE 3: Average Red-Shifts and Standard Deviations of Transition Wavelengths (for the $S_0 \rightarrow S_1$ Transition of Pt1) Due to Basis Set Improvement and Solvation

	$\Delta\bar{\lambda}$ (nm)	σ (nm)
aug-cc-pVDZ basis set for carbons	14.547	1.877
THF solvent, SCRF model	0.905	0.267

With respect to the experimental conditions, we will refer to results obtained in THF solution. The indirect effects of the solvent on the chromophore absorption spectrum as due to structure relaxation are of course accounted for in our MD/QM approach, but the direct effects as due to the polarization of the solvent are not accounted for. This latter effect is typically modeled by a reaction field of a dielectric medium in which the solute is embedded in a cavity. We have adopted this approach and determined the direct solvation effects on the $S_0 \rightarrow S_1$ transition in Pt1 for 10 randomly picked MD snapshots. It turns out that, with the nonequilibrium reaction field model, we predict a solvation red-shift as small as 0.9 nm for the dominant absorption band of Pt1 in THF, see Table 3. The standard deviation for this set of results is only 0.3 nm. So while there is a systematic shift due to the solvent, it appears to be very small. More sophisticated cavity shapes could be employed in this study, but, since the effect is so small, we decided to settle for this estimate that was obtained using a spherical cavity.

While the Pt1 chromophore consists of 131 atoms, for which the quantum chemical OPA calculations can easily be carried out, the MD simulations uses the dendrimer-coated version of Pt1, denoted by Pt1-G5, which is substantially larger. The added five generations of dendrimers increases the number of atoms to 1067, which is too large to carry out quantum chemical OPA calculation for hundreds of MD snapshots. However, experimental results show only a slight redshift of 5 nm when one generation of the dendrimer is appended to Pt1 (this molecule is referred to as Pt1-G1), but no additional shifts appear with the addition of further generations (up to Pt1-G4). We have included the experimental absorption spectrum for Pt1-G4 (as provided to us by Lindgren[55]) as an inset to Figure 3. So it is therefore well motivated to include only the first generation of dendrimer in the calculations of optical absorption spectra, and we note that the theoretical red-shift in absorption maximum in going from Pt1 to Pt1-G1 is predicted to be 6 nm (see Table 2) which is in excellent agreement with experiment. Our calculations of OPA spectra for the MD snapshots of Pt1-G5 in THF will thus be performed by first suppressing the solvent and then cutting out the first generation core of the molecule. The dangling bonds in the oxygens of the denritic units (marked by Y in Figure 2) are taken care of by the adding of hydrogens at an appropriate O−H bond length. The hereby obtained spectra are finally red-shifted by 15 nm to account for the discussed systematic shifts associated with basis set errors and solvent polarization.

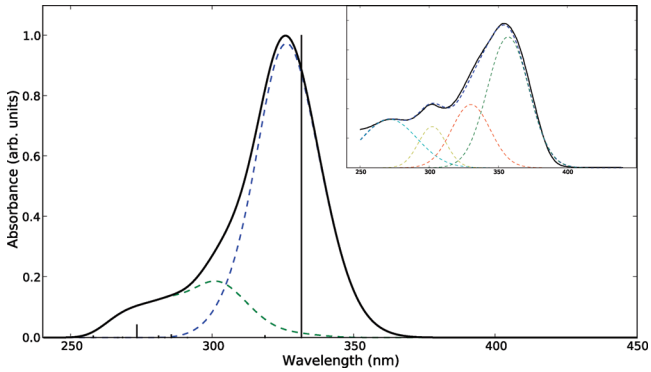

Figure 3. Averaged (over 400 MD snapshots) linear absorption spectrum including the 10 lowest singlet excited states of Pt1-G5 in THF solvent. Contributions from the first excited state and the following nine are plotted separately using dashed lines. Bars show the 10 lowest excited states, with associated oscillator strengths, for the B3LYP-optimized structure of Pt1. The inset shows the experimental absorption spectrum for low concentration Pt1-G4 in THF solvent (solid line). The experimental spectrum has been fitted to four Gaussian functions representing separate absorption bands (dashed lines).

C. Averaged Spin-Allowed and Spin-Forbidden Transition Spectra. Figure 3 shows the theoretical spin-allowed absorption spectrum of Pt1-G5 in THF—the spectrum represents an average made for 400 snapshots of a 200 ps long MD simulation. The first absorption band, which is due to the dominating $S_0 \rightarrow S_1$ transition, is separated out from others, and this absorption band decomposition is illustrated by dashed lines in the figure. The onset of the theoretical absorption spectrum is predicted to occur at around 360 nm and the band maximum is found at 325 nm. A conventional calculation of the absorption spectrum would determine transition wavelengths and oscillator strengths at the optimized geometry and then create an absorption spectrum by an ad hoc broadening of peaks. Such a procedure would in the present case have been based on the transition wavelength of 316 nm (and oscillator strength of 4.19) for Pt1-G1 that is reported in Table 2, which, after the employed red-shift of 15 nm, would lead to a band maximum at 331 nm. So the conformational averaging amounts to a shift in λ_{max} of 6 nm as compared a single-point calculation at the optimized geometry.

All things considered, it may appear discouraging to weigh the amount of work behind a conformationally averaged absorption spectrum to that behind a spectrum based on a single-point geometry when, in the end, the main result in terms of band maxima differ by a mere 6 nm. There is reason to believe, however, that the single-point approach is more error-proned than what the current example reveals. In our previous work, for example, we showed that there is another local minimum on the potential energy surface for which the normals of the planes of the phenyl rings are perpendicular to the P−Pt−P bond axis (in Figure 1 they are parallel).[21] The energy difference between the two conformations is as small as 0.8 kcal/mol (in favor of the structure in Figure 1),[21] and so which of the two minima an optimization ends up in depends mostly on the starting point for the optimization. The difference in the absorption properties between the two conformations are large; transition wavelengths differ by as much as 30 nm and oscillator strengths by close to 20%.[21] It is clear that simulations of chromophore absorption spectra based on single-point geometries risk the chance of being misrepresentative.

The experimental results for absorption onset and band maximum are 390 and 355 nm, respectively, and there is thus a discrepancy of some 30 nm between theory and experiment. We believe that this discrepancy does not originate from physical model approximations but rather from the less-than-perfect description of electron correlation in the time-dependent electron density. We have chosen to base the response theory calculations on the use of the Coulomb attenuated B3LYP exchange-correlation functional, which we, at the present time, believe is as good a description of electron correlation as is available (within the adiabatic time-dependent Kohn−Sham approximation). It was shown in ref 21 that there is a large red-shift in the absorption band maximum (c.a. 50−60 nm) associated with the adoption of the B3LYP functional, so the experimental value

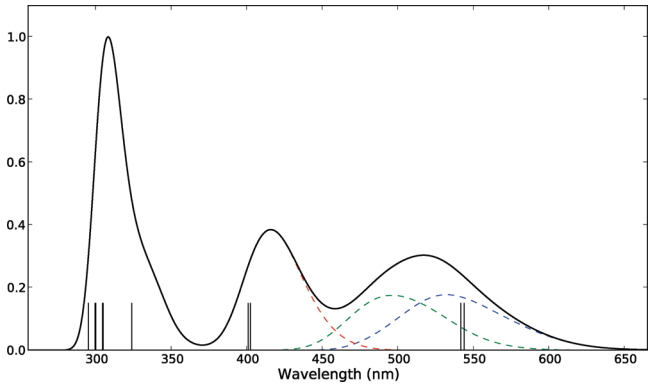

Figure 4. Averaged (over 400 MD snapshots) transition wavelengths of the 10 lowest triplet excited states of Pt1-G5 in THF solvent. Contributions from the first, second, and the following eight states are plotted separately using dashed lines. Bars show the 10 first excited states for the B3LYP-optimized structure of Pt1.

for λ_{max} falls well within the region of results that can be obtained with use of different standard functionals. We wish, however, not to enter a situation of functional-to-system (and property) fitting, and we therefore acknowledge the found error in λ_{max} but, at the same time, believe that very useful information can be obtained from systematic theoretical calculations in the work of chromophore-to-optical property optimization.

The experimental absorption spectrum for Pt1-G4 is shown as the solid curve in the inset of Figure 3. To this curve we fit four Gaussian functions as shown by the dashed lines in the inset. The main absorption peak is associated with the two rightmost Gaussian functions, which becomes separated by 27 nm after the fitting procedure is carried out. In the main figure (showing our theoretical spectrum), the separation of the peaks of the two dashed curves is 25 nm. The theoretical band separation is thus in close agreement with the separation of fitted Gaussian functions in the experiment, and we therefore believe that the attribution of two absorption bands to the main experimental absorption peak is a reasonable one. The full-width half-maximum (fwhm) broadening of the main absorption band (the $S_0 \rightarrow S_1$ transition) is, from the curve fit, found to be 35 nm, whereas that in the theoretical spectrum it is equal to 26 nm. We believe that, under the given circumstances, the agreement is satisfactory, and we attribute the discrepancy as due to a lower integrated absorption cross section of the $S_0 \rightarrow S_n$ transitions ($n > 1$) in the theoretical spectrum as compared to the experimental one.

For the spin-forbidden transition, we are, at the present level of theory, able only to determine transition wavelengths (since the corresponding oscillator strengths are zero without inclusion of valence spin−orbit interactions). What we can accomplish is something like a density of triplet states averaged over molecular conformations in the ground state, and this results in the plot in Figure 4. To be precise, the "spectral" curve is obtained by performing a Gaussian broadening (like for the singlet states) with the use of unit oscillator strengths. The resulting graph is thereafter normalized to 1.0 for the dominating peak at 310 nm. It is clear that the assumption of common unit oscillator strengths for the triplet states is not a reasonable one, and the plot is therefore not to be understood as a triplet absorption spectrum but rather, as we said, a density of states distribution. To pursue calculations of the true oscillator strengths of the ground-to-triplet excited state transitions in the nonrelativistic realm would require the addition of the spin−orbit operator by means of perturbation theory. If this were done at the all-electron level, a correct screening of the spin−orbit interaction would be provided by the spin-other-orbit terms in the Breit-Pauli operator. But a consideration of all-electron spin−orbit effects by perturbation theory for an atom as heavy as platinum is not advisible and will lead to a valence electronic structure that is inferior in quality to that obtained with the use of relativistic ECPs. On the other, the use of ECP in combination with perturbational valence spin−orbit interactions requires the introduction of effective nuclear charges to compensate for the missing electron screening.[56] Benchmarking such effective nuclear charges is a nontrivial task since it requires access to either accurate experimental or other theoretical data and it therefore falls outside the scope of the present work. In the near future, however, we intend to improve some key numerical algorithms in the Dirac program[57] and address this issue at the all-electron four-component DFT level of theory.

Our result in Figure 4 can be directly compared with the excitation spectrum of Pt1-G1 reported in Figure 5 of ref 21 and more indirectly (due to Stokes shifts) with the emission spectrum reported in Figure 3 in the same work. The excitation spectrum is recorded at 525 nm and shows (at high chromophore concentrations) broad triplet state absorption in the region of $\lambda > 400$ nm.[21] Two spectral bands can be discerned in the region between 450 and 500 nm,[21] which we attribute to the two first bands in the calculation (illustrated by dashed lines in Figure 4). The two bands lowest in energy are well separated from the other eight included in the calculations, and it is therefore possible to separate out these two in the figure. But it is noteworthy how large the discrepancy is between transition wavelengths obtained at the optimized geometry (represented by the bars in the figure) and band maxima obtained after conformational averaging. For the second band this discrepancy amounts to about 40 nm and for the third band (which is due to the third and fourth electronic state) the discrepancy is about 20 nm. These observations emphasizes the importance of conformational averaging for simulations of optical properties of chromophores with low torsional barriers.

V. Conclusions

We report MM3 force field parameters needed for molecular dynamics simulations of platinum(II) organic compounds. In accordance with most compounds reported in the literature, the heavy atom center is assumed to be in a planar configuration with two phosphine and two ethynyl ligands. The force field parameters are obtained by fits to the B3LYP potential energy surface and include bond stretch, angle bend, and torsional contributions.

The derived parameters are employed in a study of the linear absorption spectrum of a dendrimer coated platinum(II)organic molecule in THF solvent at room temperature. The broadening due to conformational averaging of the dominating $S_0 \rightarrow S_1$ absorption band is seen to have a full-width at half-maximum 26 nm, and the spectral peak at 326 nm is separated by 6 and 36 nm, respectively, from the transition wavelengths obtained at the two nearly degenerate minima on the ground state potential energy surface that are associated with ligand rotations. This observation calls for caution when one performs simulations of optical properties of chromophores with low torsional barriers.

Acknowledgment. The authors are grateful to Professor M. Lindgren at NTNU, Norway, for the provision of experimental absorption spectra. P. N. acknowledges financial support from the Swedish Research Council (Grant No. 621-2007-5269). The

authors acknowledge a grant for computing time at National Supercomputer Centre (NSC), Sweden.

Supporting Information Available: Comparison of potential energy surfaces for distortions of individual bond stretch, angle bend and torsion interactions, computed using B3LYP and MM3 with derived parameters. This material is available free of charge via the Internet at http://pubs.acs.org.

References and Notes

(1) Beljonne, D.; Wittmann, H. F.; Köhler, A.; Graham, S.; Younus, M.; J, L.; Raithby, P. R.; Khan, M. S.; Friend, R. H.; Brédas, J.-L. *J. Chem. Phys.* **1996**, *105*, 3868–3877.

(2) McKay, T. J.; Bolger, J. A.; Staromlynska, J.; Davy, J. R. *J. Chem. Phys.* **1998**, *108*, 5537.

(3) Norman, P.; Cronstrand, P.; Ericsson, J. *Chem. Phys.* **2002**, *285*, 207–220.

(4) Emmert, L. A.; Choi, W.; Marshall, J. A.; Yang, J.; Meyer, L. A.; Brozik, J. A. *J. Phys. Chem. A* **2003**, *107*, 11340–11346.

(5) Baev, A.; Rubio-Pons, O.; Gel'mukhanov, F.; Ågren, H. *J. Phys. Chem. A* **2004**, *108*, 7406–7416.

(6) Jones, S. C.; Coropceanu, V.; Barlow, S.; Kinnibrugh, T. *Organometallics* **2004**, 11782–11783.

(7) Cooper, T. M.; Hall, B. C.; Burke, A. R.; Rogers, J. E.; McLean, D. G.; Slagle, J. E.; Fleitz, P. A. *Chem. Mater.* **2004**, *16*, 3215–3217.

(8) Cooper, T. M.; Hall, B. C.; Mclean, D. G.; Rogers, J. E.; Burke, A. R.; Turnbull, K.; Weisner, A.; Fratini, A.; Liu, Y.; Schanze, K. S. *J. Phys. Chem. A* **2005**, *109*, 999–1007.

(9) Danilov, O. D.; Pomestchenko, I. E.; Kinayyigit, S.; Gentili, P. L.; Hissler, M.; Ziessel, R.; Castellano, F. N. *J. Phys. Chem. A* **2005**, *109*, 2465–2471.

(10) Schanze, K. S.; Silverman, E. E.; Zhao, X. *J. Phys. Chem. B* **2005**, *109*, 18451–18459.

(11) Zhou, G.-J.; Wong, W.-Y.; Cui, D.; Ye, C. *Chem. Mater.* **2005**, *17*, 5209–5217.

(12) Baev, A.; Norman, P.; Henriksson, J.; Ågren, H. *J. Phys. Chem. B* **2006**, *110*, 20912–20916.

(13) Cooper, T. M.; Krein, D. M.; Burke, A. R.; Mclean, D. G.; Rogers, J. E.; Slagle, J. E.; Fleitz, P. A. *J. Phys. Chem. A* **2006**, *110*, 4369–4375.

(14) Cardolaccia, T.; Funston, A. M.; Kose, M. E.; Keller, J. M.; Miller, J. R.; Schanze, K. S. *J. Phys. Chem. B* **2007**, *111*, 10871–10880.

(15) Glimsdal, E.; Carlsson, M.; Eliasson, B.; Minaev, B.; Lindgren, M. *J. Phys. Chem. A* **2007**, *111*, 244–250.

(16) Baev, A. *J. Nonlin. Opt. Phys. Mater* **2007**, *16*, 157–169.

(17) Samoc, M.; Dalton, G. T.; Gladysz, J. A.; Zheng, Q.; Velkov, Y.; Ågren, H.; Norman, P.; Humphrey, M. G. *Inorg. Chem.* **2008**, *47*, 9946.

(18) Yang, Z.-D.; Feng, J.-K.; Ren, A.-M. *Inorg. Chem.* **2008**, *47*, 10841–10850.

(19) Ramakrishna, G.; Goodson III, T.; Rogers-Haley, J. E.; Cooper, T. M.; McLean, D. G.; Urbas, A. *J. Phys. Chem. C* **2009**, *113*, 1060–1066.

(20) Keller, J. M.; Schanze, K. S. *Organometallics* **2009**, *28*, 4210–4216.

(21) Glimsdal, E.; Norman, P.; Lindgren, M. *J. Phys. Chem. A* **2009**, *113*, 11242−11249.

(22) Chan, S.-C.; Chan, M. C. W.; Wang, Y.; Che, C.-M.; Cheung, K.-K.; Zhu, N. *Chem.—Eur. J.* **2001**, *7*, 4180–4190.

(23) Sun, W.; Wu, Z.-X.; Yang, Q.-Z.; Wu, L.-Z.; Tung, C.-H. *Appl. Phys. Lett.* **2003**, *82*, 850.

(24) Jude, H.; Krause Bauer, J. A.; Connick, W. B. *J. Am. Chem. Soc.* **2003**, *125*, 3446.

(25) Zhang, D.; Wu, L.-Z.; Yang, Q.-Z.; Li, X.-H.; Zhang, L.-P.; Tung, C.-H. *Opt. Lett.* **2003**, *5*, 3221.

(26) Wong, K. M.-C.; Tang, W.-S.; Chu, B. W.-K.; Zhu, N.; Yam, V. W.-W. *Organometallics* **2004**, *23*, 3459–3465.

(27) Rogers, J. E.; Slagle, J. E.; Krein, D. M.; Burke, A. R.; Hall, B. C.; Fratini, A.; McLean, D. G.; Fleitz, P. A.; Cooper, T. M.; Drobizhev, M.; Makarov, N. S.; Rebane, A.; Kim, K.-Y.; Farley, R.; Schanze, K. S. *Inorg. Chem.* **2007**, *46*, 6483–94.

(28) Zhou, G.-J.; Wong, W.-Y.; Ye, C.; Lin, Z. *Adv. Funct. Mater.* **2007**, *17*, 963–975.

(29) Westlund, R.; Malmström, E.; Lopes, C.; Öhgren, J.; Rodgers, T.; Saito, Y.; Kawata, S.; Glimsdal, E.; Lindgren, M. *Adv. Funct. Mater.* **2008**, *18*, 1939–1948.

(30) Mei, J.; Ogawa, K.; Kim, Y.-G.; Heston, N. C.; Arenas, D. J.; Nasrollahi, Z.; McCarley, T. D.; Tanner, D. B.; Reynolds, J. R.; Schanze, K. S. *Appl. Mater. Interfaces* **2009**, *1*, 150–161.

(31) Chawdhury, N.; Köhler, A.; Friend, R. H.; Wong, W.-Y.; Lewis, J.; Younus, M.; Raithby, P. R.; Corcoran, T. C.; Al-Mandhary, M. R. A.; Khan, M. S. *J. Chem. Phys.* **1999**, *110*, 4963.

(32) Wilson, J. S.; Dhoot, A. S.; Seeley, A. J.; Khan, M. S.; Köhler, A.; Friend, R. H. *Nature* **2001**, *413*, 828–831.

(33) Köhler, A.; Wilson, J. *Org. Elect.* **2003**, *4*, 179–189.

(34) Baldo, M. A.; O'Brien, D. F.; You, Y.; Shoustikov, A.; Sibley, S.; Thompson, M. E.; Forrest, S. R. *Nature* **1998**, *395*, 151–154.

(35) Guo, F.; Kim, Y.-G.; Reynolds, J. R.; Schanze, K. S. *Chem. Commun.* **2006**, 1887–1889.

(36) Liu, Y.; Jiang, S.; Glusac, K.; Powell, D. H.; Anderson, D. F.; Schanze, K. S. *J. Am. Chem. Soc.* **2002**, *124*, 12412–3.

(37) Norman, P.; Ågren, H. *J. Comp. Theor. Nanoscience* **2005**, *1*, 343.

(38) Allinger, N. L.; Yuh, Y. H.; Lii, J. *J. Am. Chem. Soc.* **1989**, *111*, 8551.

(39) Allinger, N. L.; Li, F.; Tai, J. C. *J. Comput. Chem.* **1990**, *11*, 868–895.

(40) Calus, S.; Gondek, E.; Danel, A.; Jarosz, B.; Kityk, A. *Opt. Commun.* **2006**, *268*, 64.

(41) Kongsted, J.; Osted, A.; Mikkelsen, K. V.; Åstrand, P.-O.; Christiansen, O. *J. Chem. Phys.* **2004**, *121*, 8435.

(42) Becke, A. D. *J. Chem. Phys.* **1993**, *98*, 5648.

(43) Frisch, M. J.; Trucks, G. W.; Schlegel, H. B.; Scuseria, G. E.; Robb, M. A.; Cheeseman, J. R.; Montgomery, Jr., J. A.; Vreven, T.; Kudin, K. N.; Burant, J. C.; Millam, J. M.; Iyengar, S. S.; Tomasi, J.; Barone, V.; Mennucci, B.; Cossi, M.; Scalmani, G.; Rega, N.; Petersson, G. A.; Nakatsuji, H.; Hada, M.; Ehara, M.; Toyota, K.; Fukuda, R.; Hasegawa, J.; Ishida, M.; Nakajima, T.; Honda, Y.; Kitao, O.; Nakai, H.; Klene, M.; Li, X.; Knox, J. E.; Hratchian, H. P.; Cross, J. B.; Bakken, V.; Adamo, C.; Jaramillo, J.; Gomperts, R.; Stratmann, R. E.; Yazyev, O.; Austin, A. J.; Cammi, R.; Pomelli, C.; Ochterski, J. W.; Ayala, P. Y.; Morokuma, K.; Voth, G. A.; Salvador, P.; Dannenberg, J. J.; Zakrzewski, V. G.; Dapprich, S.; Daniels, A. D.; Strain, M. C.; Farkas, O.; Malick, D. K.; Rabuck, A. D.; Raghavachari, K.; Foresman, J. B.; Ortiz, J. V.; Cui, Q.; Baboul, A. G.; Clifford, S.; Cioslowski, J.; Stefanov, B. B.; Liu, G.; Liashenko, A.; Piskorz, P.; Komaromi, I.; Martin, R. L.; Fox, D. J.; Keith, T.; Al-Laham, M. A.; Peng, C. Y.; Nanayakkara, A.; Challacombe, M.; Gill, P. M. W.; Johnson, B.; Chen, W.; Wong, M. W.; Gonzalez, C.; Pople, J. A. Gaussian 03, Revision C.02; Gaussian, Inc.: Wallingford, CT, 2004.

(44) Hehre, W. J.; Ditchfield, R.; Pople, J. A. *J. Chem. Phys.* **1972**, *56*, 2257.

(45) Harihan, P. C.; Pople, J. A. *Theor. Chim. Acta.* **1973**, *28*, 213.

(46) Bergner, A.; Dolg, M.; Küchle, W.; Stoll, H.; Preuss, H. *Mol. Phys.* **1993**, *80*, 1431.

(47) Andrae, D.; Häussermann, U.; Dolg, M.; Stoll, H.; Preuss, H. *Theor. Chim. Acta.* **1990**, *77*, 123.

(48) Ponder, J. W. *TINKER, Ver. 4.2*; 2004; http://dasher.wustl.edu/tinker.

(49) Berendsen, H. J. C.; Postma, J. P. M.; van Gunsteren, W. F.; DiNola, A.; Haak, J. R. *J. Chem. Phys.* **1984**, *81*, 3684.

(50) *DALTON, A Molecular Electronic Structure Program, Release 2.0*; 2005; see http://www.kjemi.uio.no/software/dalton/dalton.html.

(51) Yanai, T.; Tew, D. P.; Handy, N. C. *Chem. Phys. Lett.* **2004**, *393*, 51.

(52) Peach, M. J. G.; Helgaker, T.; Salek, P.; Keal, T. W.; Lutnæs, O. B.; Tozer, D. J.; Handy, N. C. *Phys. Chem. Chem. Phys.* **2006**, *8*, 558.

(53) Kendall, R. A.; Dunning, T. H., Jr.; Harrison, R. J. *J. Chem. Phys.* **1992**, *96*, 6796.

(54) Mikkelsen, K. V.; Ågren, H.; Jensen, H. J. A.; Helgaker, T. *J. Chem. Phys.* **1988**, *89*, 3086.

(55) Lindgren, M. Private communication, 2009.

(56) Jansson, E.; Norman, P.; Minaev, B.; Ågren, H. *J. Chem. Phys.* **2006**, *124*, 114106.

(57) Visscher, L.; Jensen, H. J. A.; Saue, T.; Bast, R.; Dubillard, S.; Dyall, K. G.; Ekström, U.; Eliav, E. T.; Fleig, E.; Gomes, A. S. P.; Helgaker, T. U.; Henriksson, J.; Ilias, M.; Jacob, C. R.; Knecht, S.; Norman, P.; Olsen, J.; Pernpointner, M.; Ruud, K.; Salek, P.; Sikkema, J. *DIRAC, A Relativistic ab Initio Electronic Structure Program, Release DIRAC08*; 2008; see http://dirac.chem.sdu.dk.

JP911046U